Electronic Supplementary Information

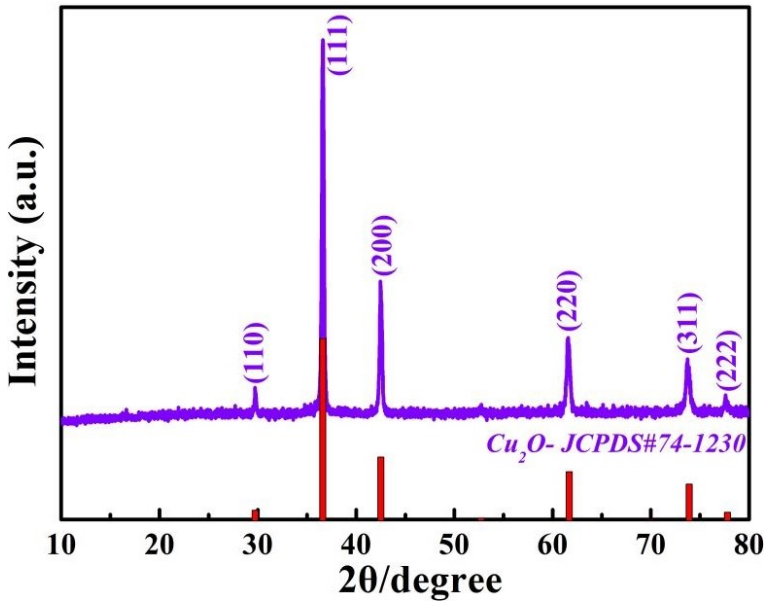

Fig. S1 XRD pattern of the Cu_2O microcubes.

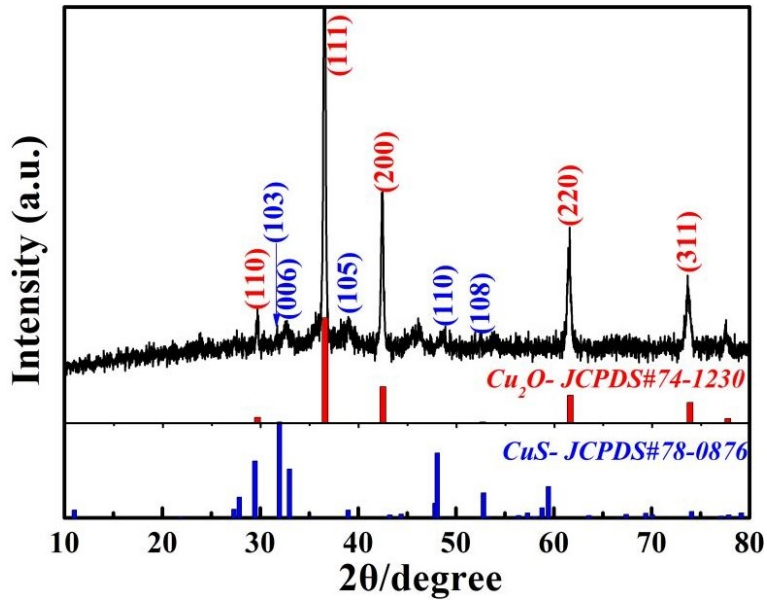

Fig. S2 XRD pattern of the Cu_2O@CuS microcubes.

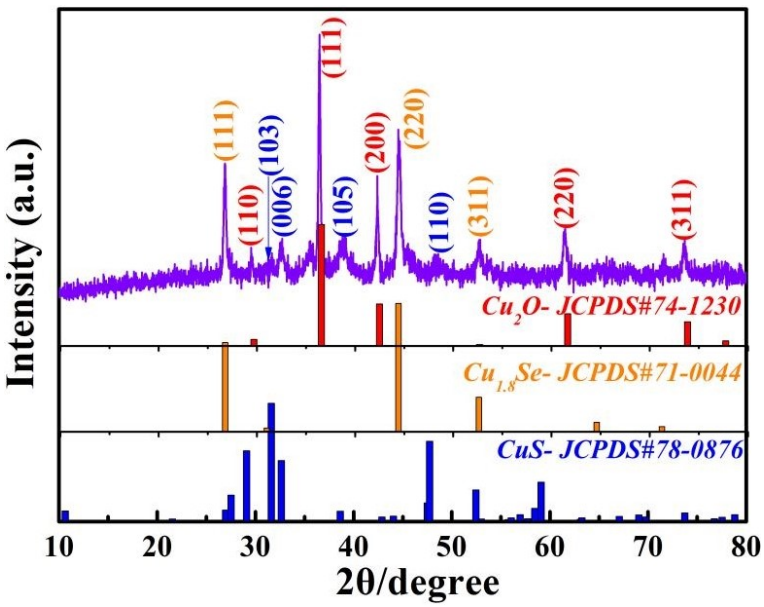

Fig. S3 XRD pattern of the Cu_2O@CuS@$Cu_{1.8}Se$ microcubes.

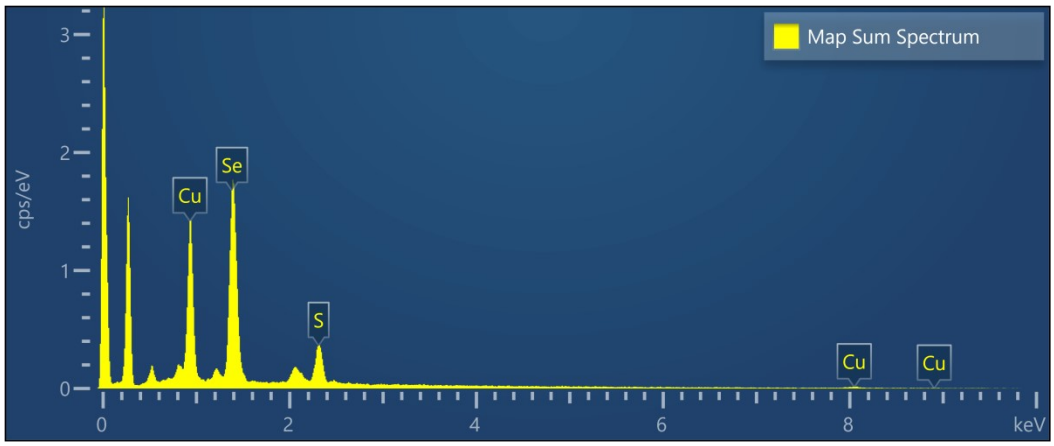

Fig. S4 EDX spectrum of the CuS@CuSe microcubes

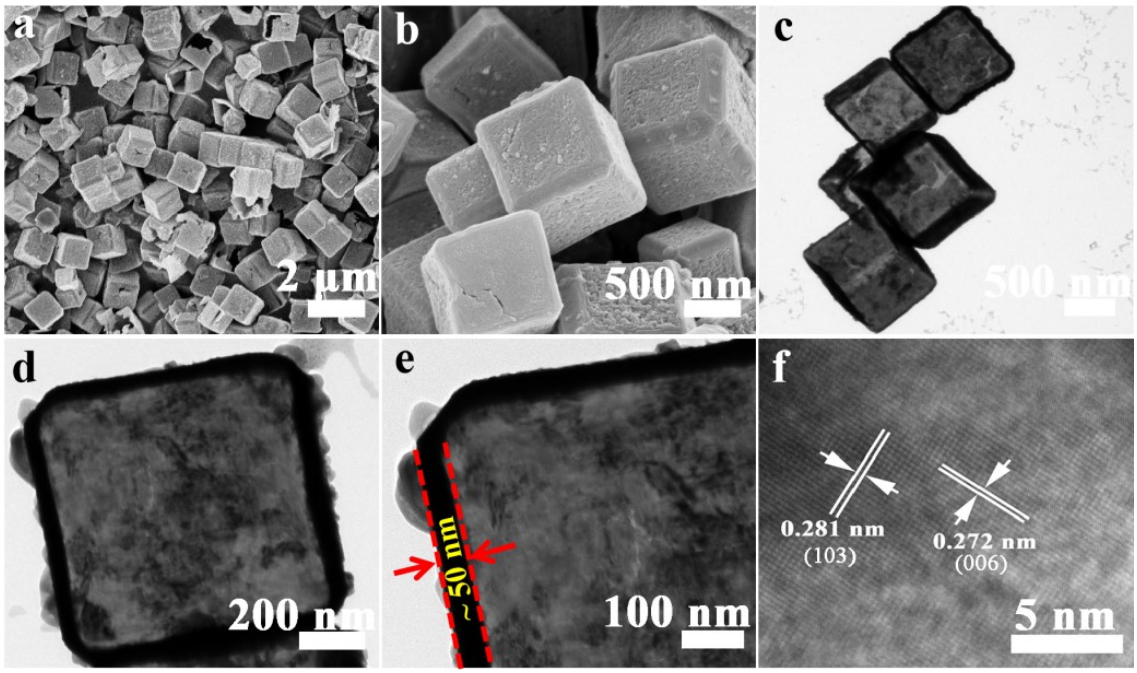

Fig. S5 Structural characterizations of the CuS microcubes: (a, b) SEM images, (c-e) TEM images, (f) HRTEM image.

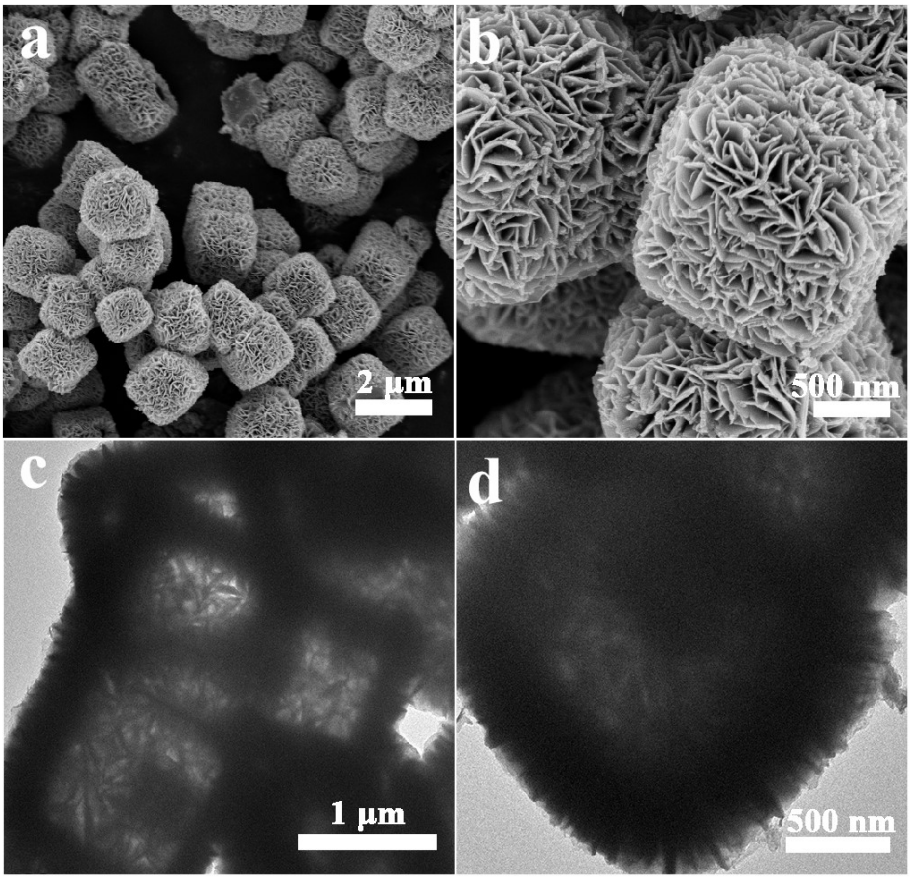

Fig. S6 Structural characterizations of the Cu_2O@CuSe microcubes: (a, b) SEM images, (c-e) TEM images.

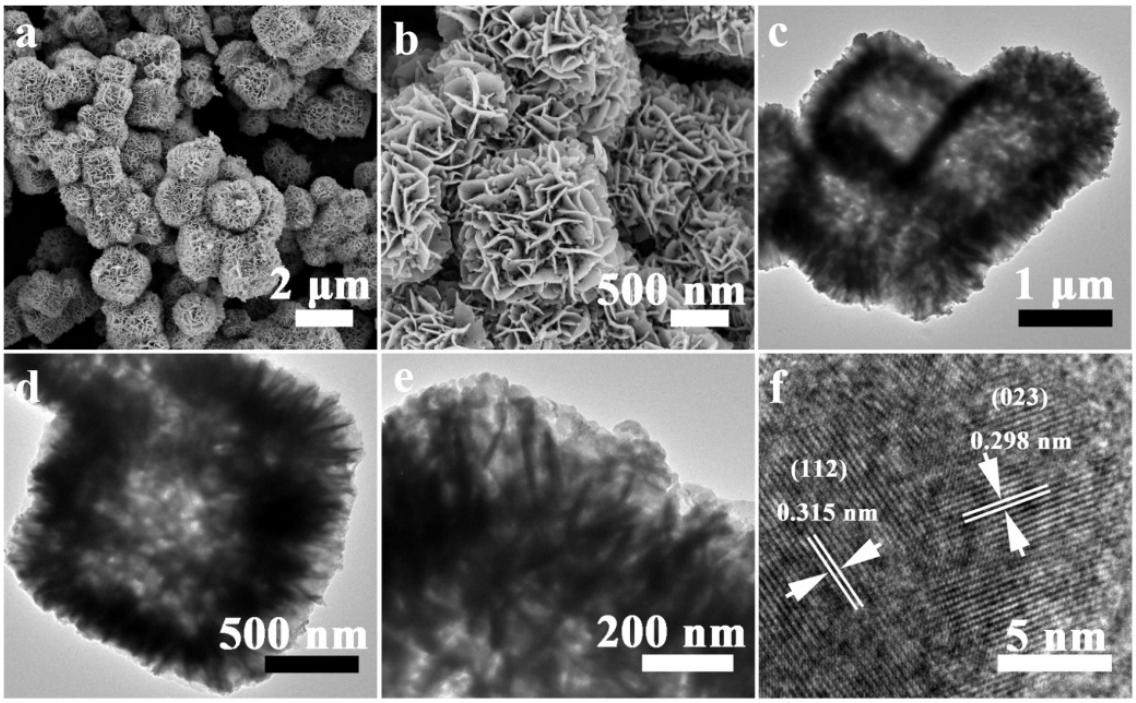

Fig. S7 Structural characterizations of the CuSe microcubes: (a, b) SEM images, (c-e) TEM images, (f) HRTEM image.

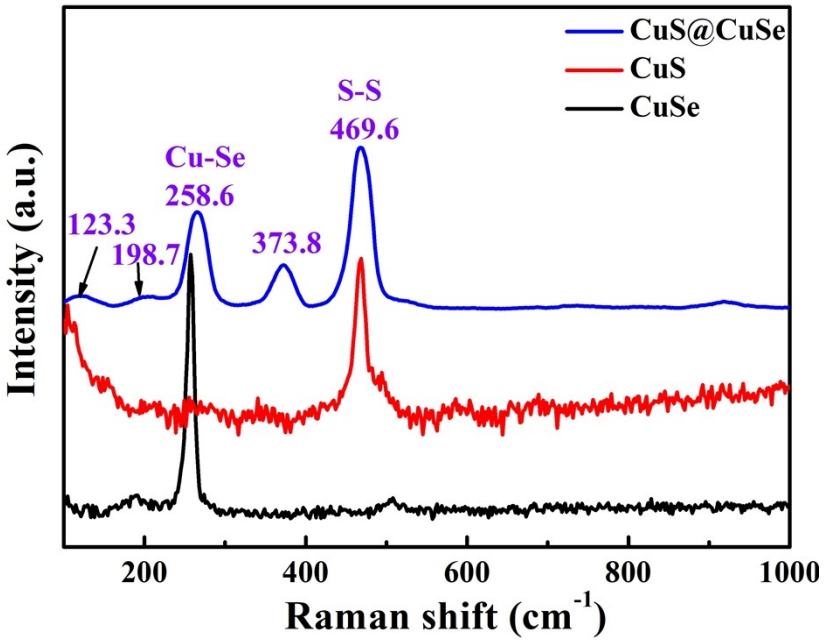

Fig. S8 Raman spectra of the CuS@CuSe, single CuS, and CuSe.

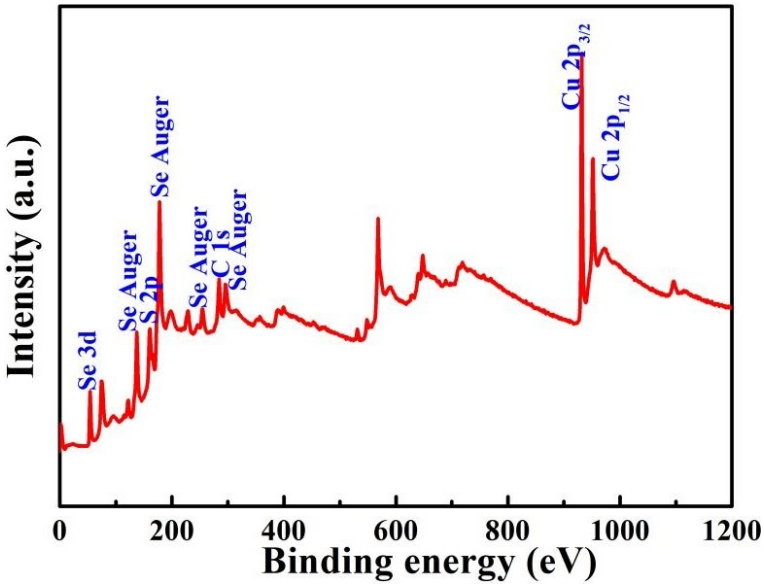

Fig. S9 XPS curvey spectrum of the CuS@CuSe microcubes.

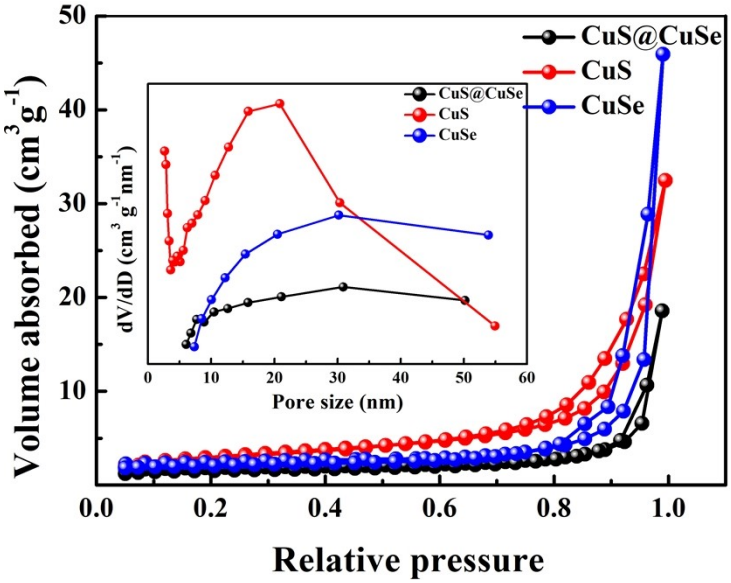

Fig. S10 Nitrogen adsorption–desorption isotherms and pore size distribution of the CuS@CuSe, single CuS, and CuSe.

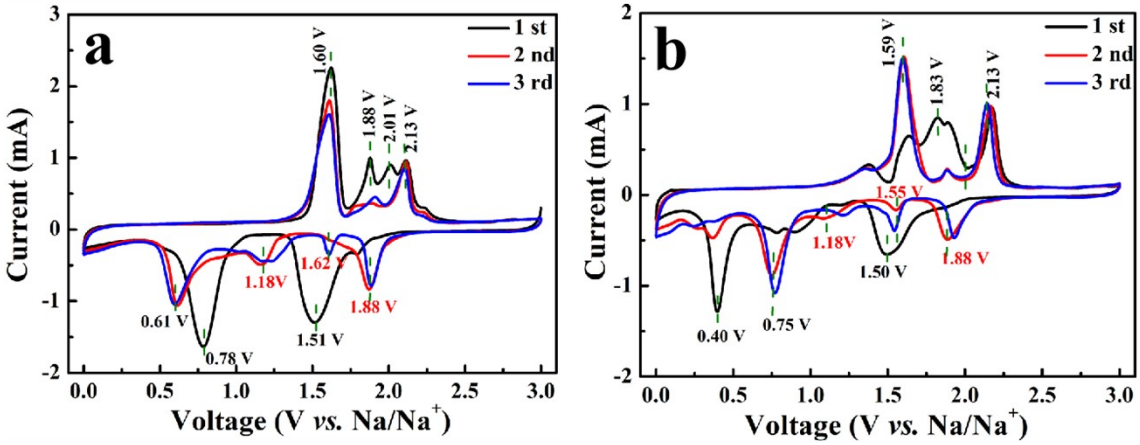

Fig. S11 CV curves of the CuS (a) and CuSe (b) electrodes at 0.5 mV s^{-1}.

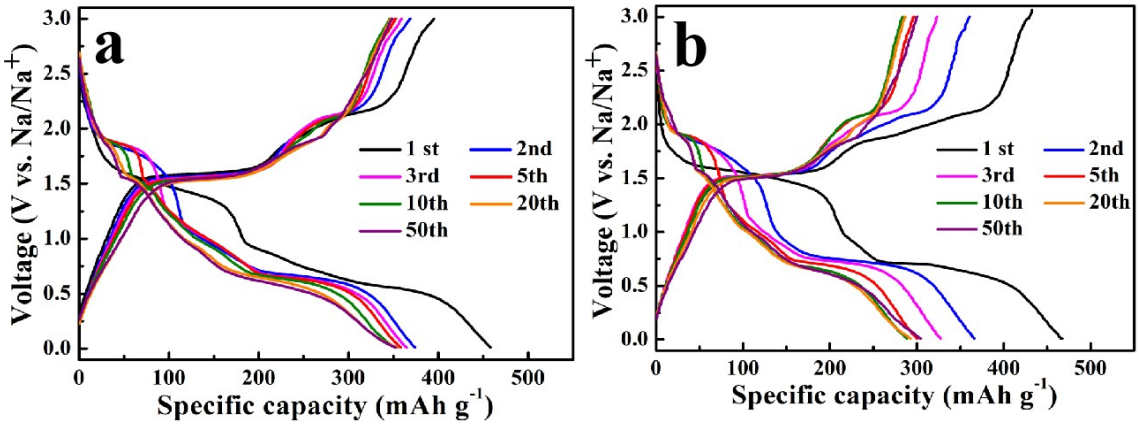

Fig. S12 GDC curves of the CuS (a) and CuSe (b) electrodes at 2.0 A g^{-1}.

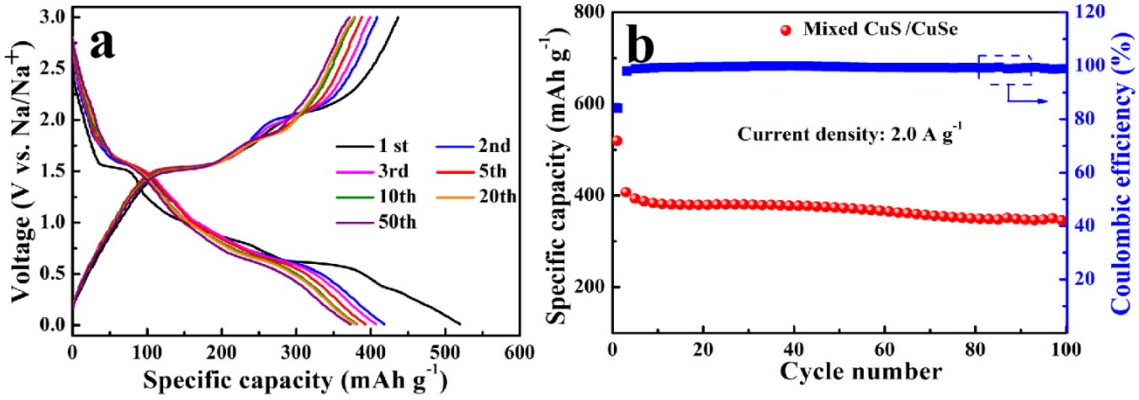

Fig. S13 GDC curves (a) and cycling performance (b) of the mixed CuS/CuSe electrode with a mass ratio of 1:1 at 2.0 A g^{-1}.

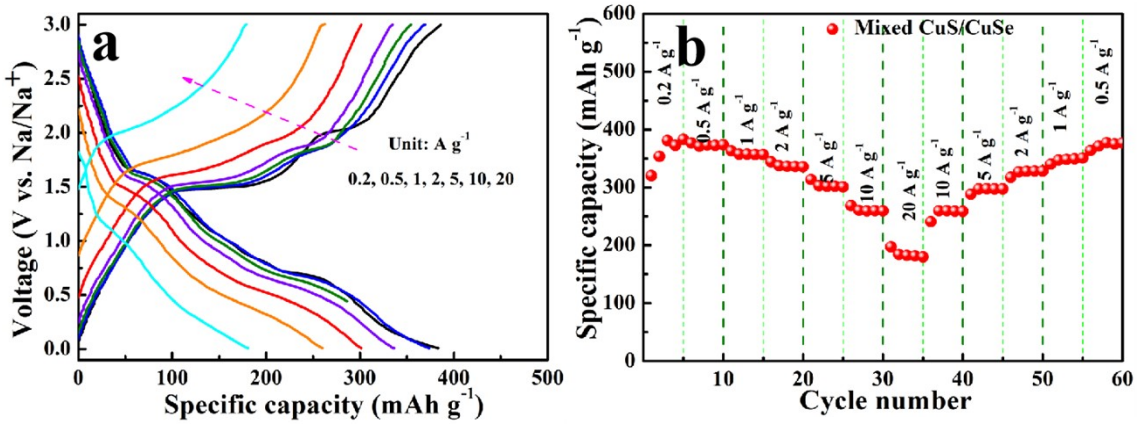

Fig. S14 GDC curves at different rates (a) and rate performance (b) of the mixed CuS/CuSe electrode with a mass ratio of 1:1.

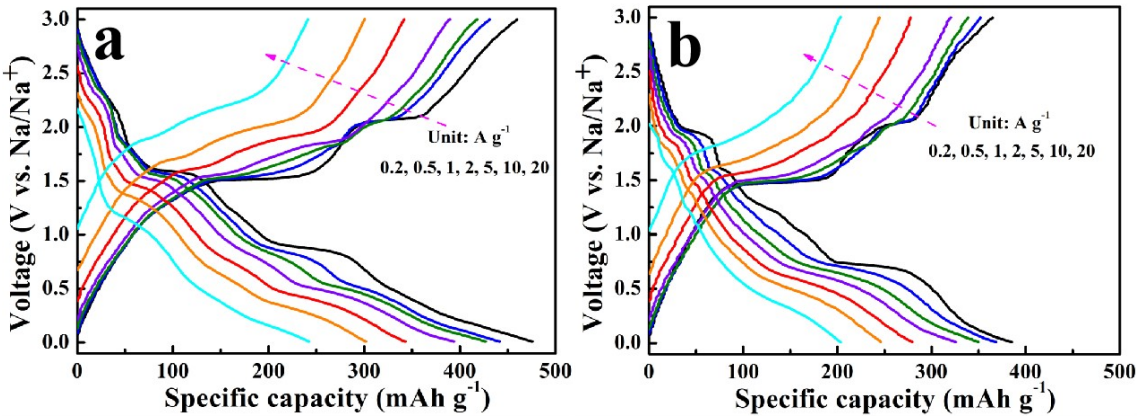

Fig. S15 GDC profiles of single CuS (a) and CuSe (b) electrodes at diverse rates.

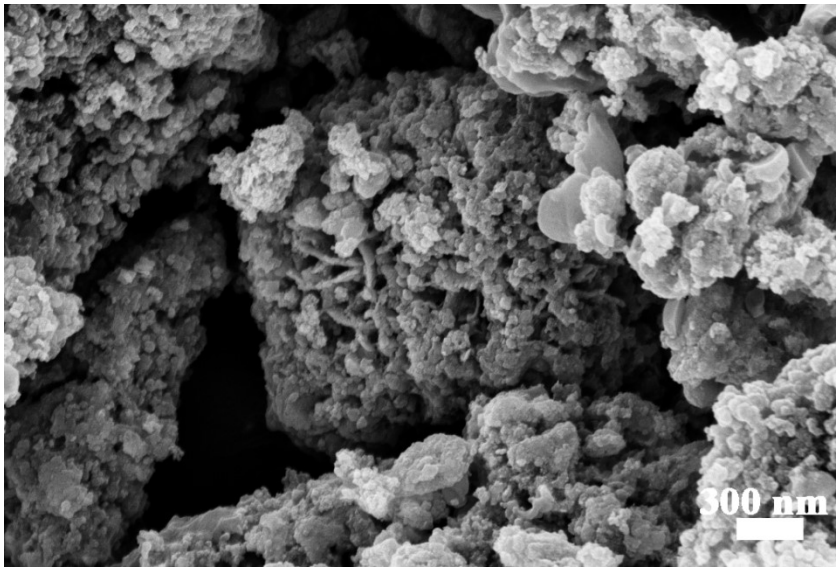

Fig. S16 SEM image of CuS@CuSe electrode after long-term cycle at 2.0 A g^{-1}.

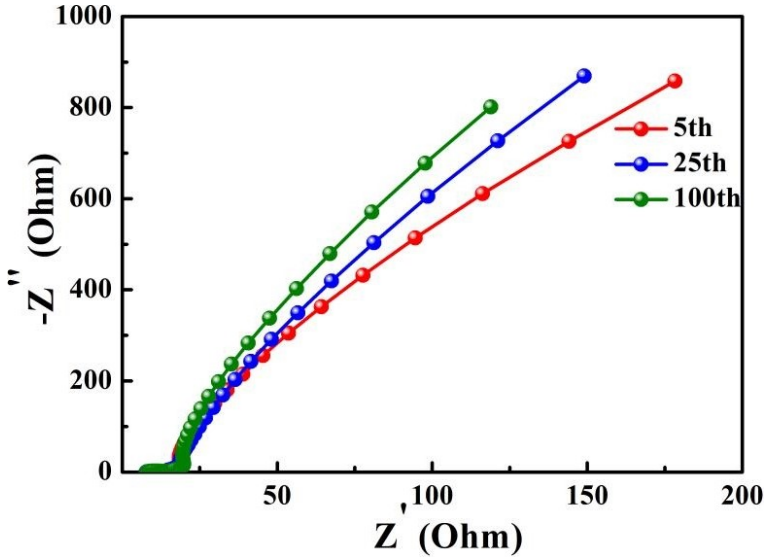

Fig. S17 Nyquist plots of the CuS@CuSe electrode at the 5th, 25th, and 50th cycle.

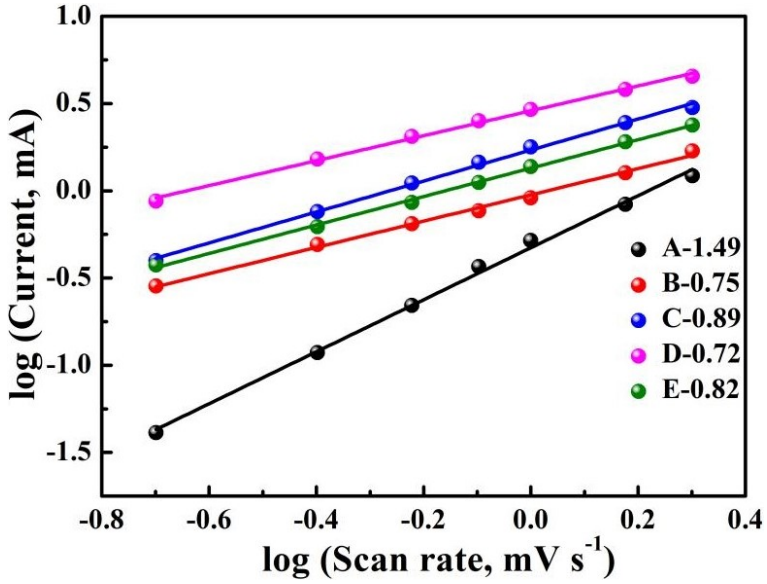

Fig. S18 The logarithmic linear plots between log *v* and log *i* at five specific redox peaks for the CuS@CuSe electrode.

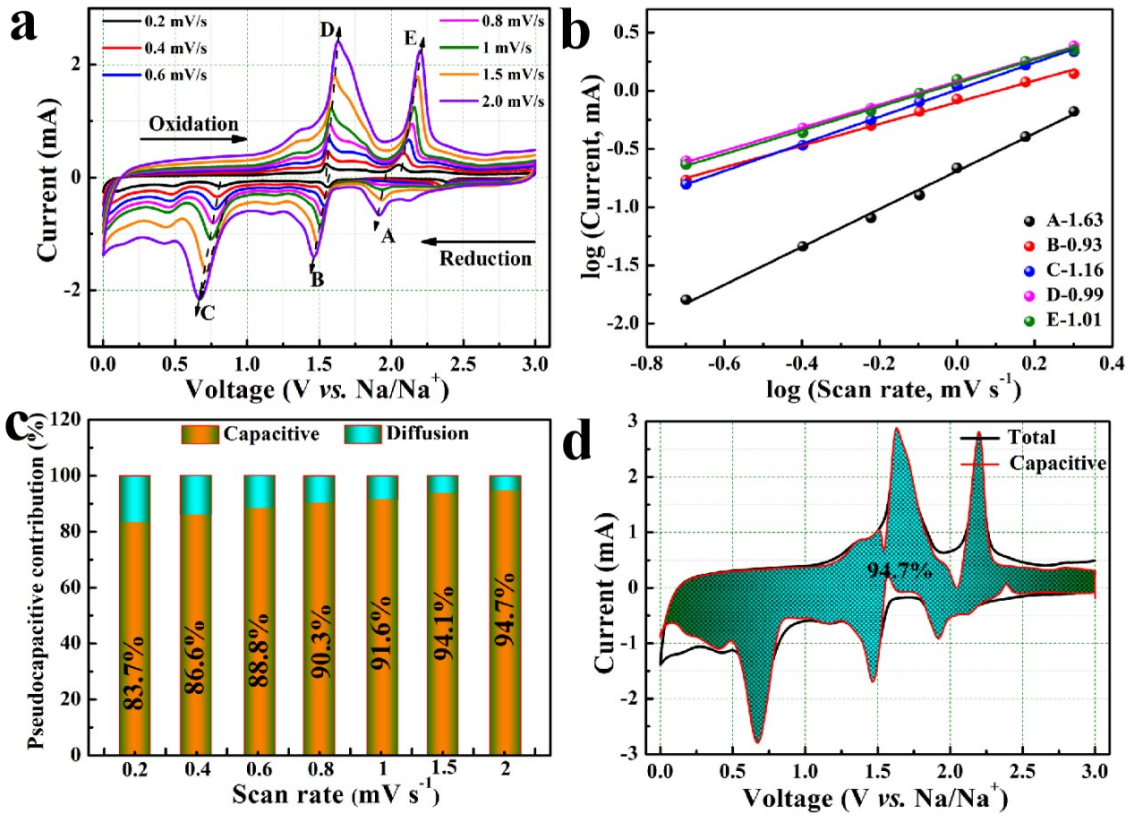

Fig. S19 CV curves (a) of the CuS electrode at diverse scan rates, and the corresponding logarithmic linear plots between log *v* and log *i* at five specific redox peaks (b). (c) Capacitive contribution of the CuS electrode conducted at 2.0 mV s^{-1}. (d) The normalized contribution proportion of the capacitive for the CuS electrode at each scan rate.

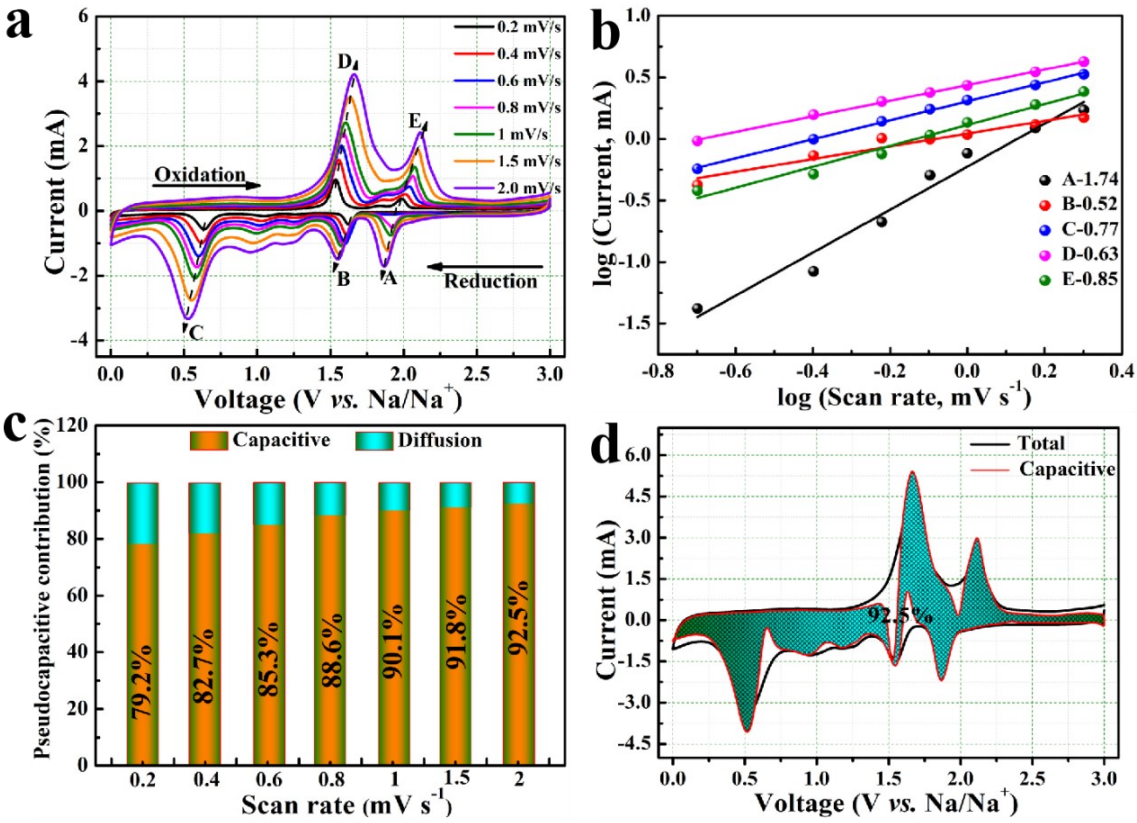

Fig. S20 CV curves (a) of the CuSe electrode at diverse scan rates, and the corresponding logarithmic linear plots between log *v* and log *i* at five specific redox peaks (b). (c) Capacitive contribution of the CuSe electrode conducted at 2.0 mV s^{-1}. (d) The normalized contribution proportion of the capacitive for the CuSe electrode at each scan rate.

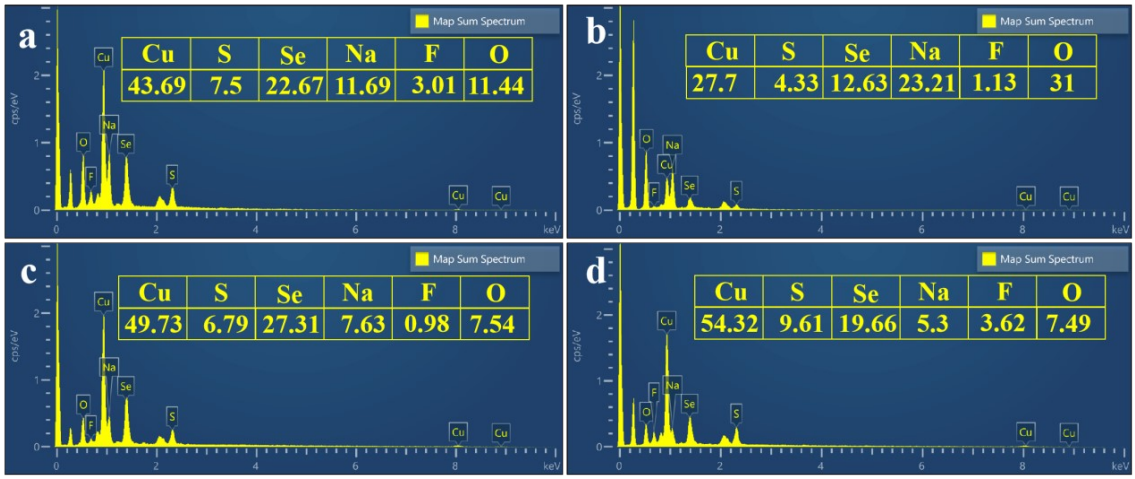

Fig. S21 Ex-situ EDX spectra at different discharged/charged states for the CuS@CuSe electrode: (a) Discharged to 1.5 V, (b) Discharged to 0.01 V, (c) Charged to 1.56 V, (d) Charged to 3.0 V.

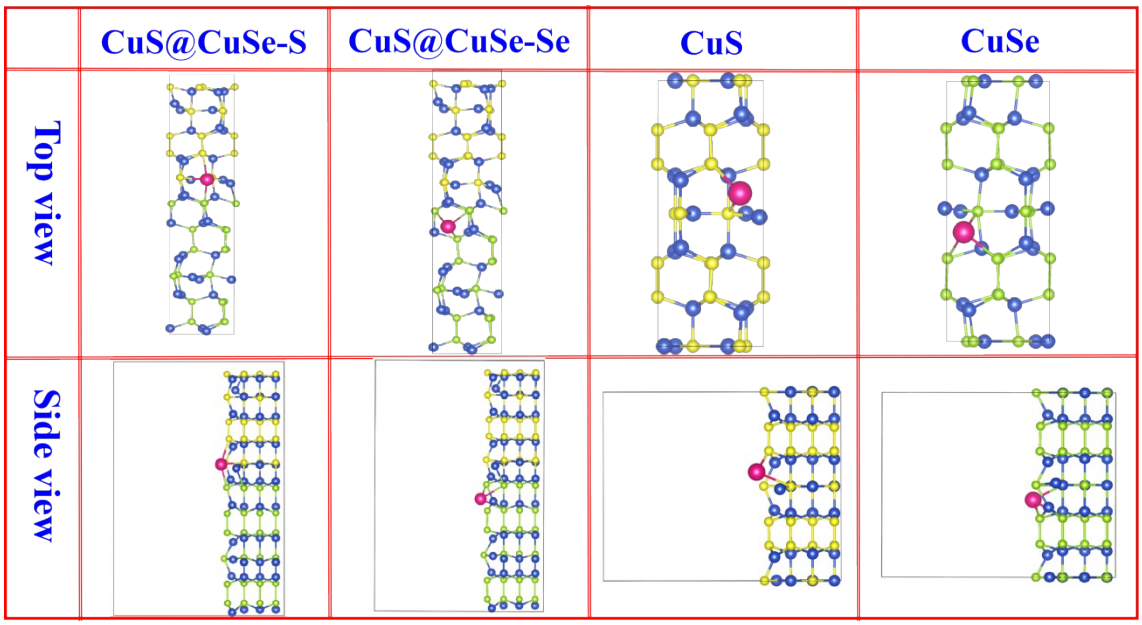

Fig. S22 Schematic illustration of Na^+ adsorbed onto CuS@CuSe, CuS, and CuSe with the top view and side view. In which CuS@CuSe-S and CuS@CuSe-Se represent Na^+ absorbed on the CuS/CuSe interface close to CuS or CuSe side, respectively.

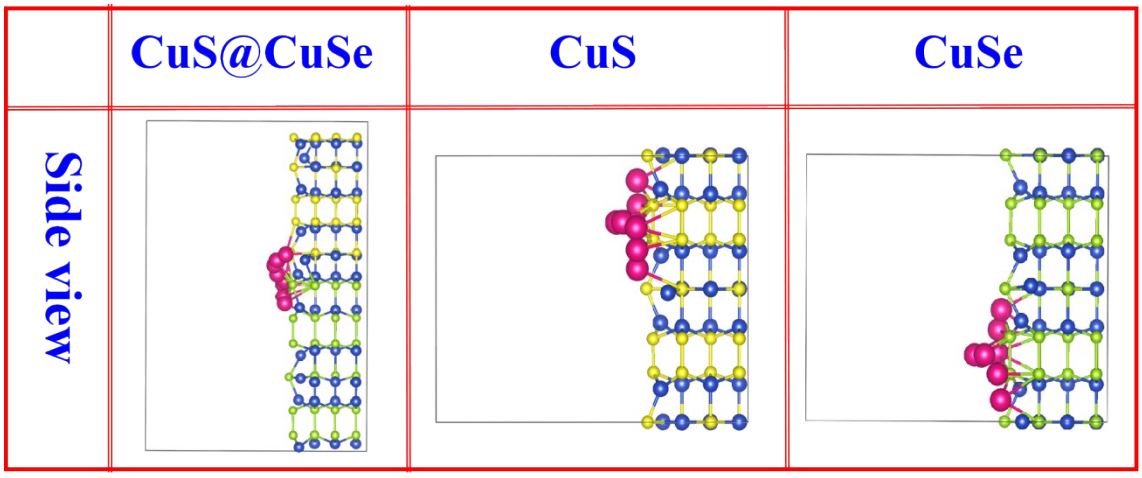

Fig. S23 Ionic migration path in CuS@CuSe, CuS, and CuSe with the side view.

Table S1 ICP analysis of the CuS@CuSe composites.

Samples	S (Wt %)	Se (Wt %)	Mass ratio	Molar ratio
CuS@CuSe	7.22	68.71	0.28 : 1	0.42 : 1

Table S2 Comparison of cycle lifespan and specific capacity of the CuS@CuSe anode with previous reported CuS-/CuSe-based anodes in SIBs systems.

Materials	Voltage window (V)	Rate (A g^{-1})	Cycle number	Capacity (mAh g^{-1})	Ref.
Nanosheets-assembled CuSe	0.4-3.0	5.0	1200	290.0	1
Micro-sized Cu_2Se	0.3-2.2	1.0	1000	256.0	2
Cu_2Se nanosheet array	0.4-3.0	20.0	6500	220.0	3
Cu_2Se-ZnSe heterojunction	0.01-3.0	0.5	500	205.0	4
Mesoporous $Cu_{2-x}Se$ nanocrystals	0.3-2.5	5.0	3000	212.4	5
Cu_2Se@N-C	0.01-3.0	2.0	2000	101.0	6
Bulk $Cu_{2-x}Se$ plates	0.4-3.0	5.0	1000	316.1	7
$Cu_{2-x}Se$ nanorods	1.0-3.0	0.1	400	149.3	8
CuS microspheres	0.4-3.0	10	1000	312.5	9
CuS microspheres	0.6-3.0	0.5	500	403.0	10
CuS@CoS_2 double-shelled nanoboxes	0.4-2.6	0.5	500	403.0	11
N-doped CuS@C nanowires	0.4-3.0	2.0	10000	216.7	12
Platelet-like CuS	0.4-2.6	2.0	500	320	13
ZnS/CuS@C	0.4-3.0	10.0	1750	282.7	14
Hydrangea-like CuS	0.4-2.6	1.0	400	335	15
Pine-needle-like CuS	0.3-3.0	5.0	1000	436.0	16
CuS@N-C	0.4-3.0	5.0	1200	300.2	17
CuS@CuSe	0.01-3.0	20.0	1500	303.1	This work

References

1 H. Z. Lin, M. L. Li, X. Yang, D. X. Yu, Y. Zeng, C. Z. Wang, G. Chen and F. Du, *Adv. Energy Mater.,* 2019, **9**, 1900323.

2 L. Y. Shao, S. G. Wang, J. P. Qi, Z. P. Sun, X. Y. Shi, Y. S. Shi and X. Lu, *Mater. Today Phys.,* 2021, **19**, 100422.

3 Y. H. Xiao, X. B. Zhao, X. Z. Wang, D. C. Su, S. Bai, W. Chen, S. M. Fang, L. M. Zhou, H. M. Cheng and F. Li, *Adv. Energy Mater.,* 2020, **10**, 2070113.

4 Q. Gao, P. C. Li, S. S. Ding, H. C. He, M. Q. Cai, X. T. Ning, Y. Cai and M. Zhang, *Ionics,* 2020, **26**, 5525–5533.

5 Y. J. Li, X. C. Sun, Z. J. Cheng, X. Xu, J. Pan, X. F. Yang, F. Tian, Y. L. Li, J. Yang and Y. T. Qian, *Energy Storage Mater.,* 2019, **22**, 275–283.

6 L. Hu, C. Q. Shang, E. M. Akinoglu, X. Wang and G. F. Zhou, *Nanomaterials,* 2020, **10**, 302.

7 Y. H. Xiao, K. Y. Zhang, X. B. Zhao, D. C. Su, L. M. Zhou, S. D. Wu, X. Z. Wang, H. Z. Guo and S. M. Fang, *J. Alloy. Compd.,* 2021, **879**, 160485.

8 H. Li, J. L. Jiang, J. X. Huang, Y. H. Wang, Y. Y. Peng, Y. Y. Zhang, B. J. Hwang and J. B. Zhao, *ACS Appl. Mater. Interfaces,* 2018, **10**, 13491–13498.

9 Y. H. Xiao, D. C. Su, X. Z. Wang, S. D. Wu, L. M. Zhou, Y. Shi, S. M. Fang, H. M. Cheng and F. Li, *Adv. Energy Mater.,* 2018, **8**, 1800930.

10 H. Li, Y. H. Wang, J. L. Jiang, Y. Y Zhang, Y. Y. Peng and J. B. Zhao, *Electrochim. Acta,* 2017, **247**, 851–859.

11 Y. J. Fang, B. Y. Guan, D. Y. Luan and X. W. Lou, *Angew. Chem., Int. Ed.,* 2019, **58**, 7739–7748.

12 D. Zhao, M. M. Yin, C. H. Feng, K. Zhan, Q. Z. Jiao, H. S. Li and Y. Zhao, *ACS Sustainable Chem. Eng.,* 2020, **8**, 11317–11327.

13 Z. G. Yang, Z. G. Wu, J. Liu, Y. X. Liu, S. Y. Gao, J. A. Wang, Y. Xiao, Y. J. Zhong, B. H. Zhong and X. D. Guo, *J. Mater. Chem. A,* 2020, **8**, 8049–8057.

14 W. X. Zhao, L. X. Gao, L. C. Yue, X. Y. Wang, Q. Liu, Y. L. Luo, T. S. Li, X. F. Shi, A. M. Asiri and X. P. Sun, *J. Mater. Chem. A,* 2021, **9**, 6402–6412.

15 Z. G. Yang, Z. G. Wu, W. B. Hua, Y. Xiao, G. K. Wang, Y. X. Liu, C. J. Wu, Y. C. Li, B. H. Zhong, W. Xiang, Y. J. Zhong and X. D. Guo, *Adv. Sci.,* 2020, **7**, 1903279.

16 D. X. Yu, M. L. Li, T. Yu, C. Z. Wang, Y. Zeng, X. D. Hu, G. Chen, G. C. Yang and F. Du, *J. Mater. Chem. A,* 2019, **7**, 10619–10628.

17 X. Q. Liu, X. Y. Li, X. L. Lu, X. He, N. Jiang, Y. Huo, C. G. Xu and D. M. Lin, *J. Alloy. Compd.,* 2021, **854**, 157132.